Physics of the Dark Universe 36 (2022) 101037

Contents lists available at ScienceDirect

Physics of the Dark Universe

journal homepage: www.elsevier.com/locate/dark

Quintessence or phantom: Study of scalar field dark energy models through a general parametrization of the Hubble parameter

Nandan Roy [a,*], Sangita Goswami [b], Sudipta Das [b]

[a] Centre for Theoretical Physics & Natural Philosophy, Mahidol University, Nakhonsawan Campus, Phayuha Khiri, Nakhonsawan 60130, Thailand
[b] Department of Physics, Visva-Bharati, Santiniketan 731235, India

ARTICLE INFO

Article history:
Received 18 March 2022
Received in revised form 26 April 2022
Accepted 3 May 2022

Keywords:
Dark energy
Hubble tension
Quintessence
Phantom

ABSTRACT

In this work we propose a simple general parametrization scheme of the Hubble parameter for the scalar field dark energy models. In our approach it is possible to incorporate both the quintessence and phantom scalar field in a single analytical scheme and write down relevant cosmological parameters which are independent of the nature of the scalar field. A general condition for the phantom barrier crossing has also been obtained. To test this approach, a well behaved parametrization of the normalized Hubble parameter has been considered and a wide variety of observational data like CMB data, Supernovae data, BAO data etc. has been used to constraint the various cosmological parameters. It has been found that data prefer the present value of the equation of state of the dark energy to be in the phantom domain. One interesting outcome of this analysis is that although the current value of the dark energy equation of state is phantom in nature, a phantom crossing of the EOS has taken place in the recent past. We have also carried out the Bayesian model comparison between ΛCDM model and the proposed model which indicates that this model is favored by data as compared to ΛCDM model.

1. Introduction

Even after two decades of its discovery, the reason behind accelerated expansion of the universe [1–5] remains a mystery. Moreover the observational data also suggest that the onset of this accelerated phase has taken place very recently, at around $z \sim 0.5$ [6,7]. If we consider the theory of gravity to be general relativity, any proposed candidate behind the accelerated expansion of the universe referred to as "dark energy" (DE) must have a sufficient negative pressure to counterbalance gravity and drive the accelerated expansion [8]. Cosmological constant (Λ), the most successful of all proposals, is however troubled by the challenges coming from both theoretical and observational sides. An alternative proposal is a dynamical DE model. Till now a variety of such DE models have been proposed, such as quintessence, k-essence, phantom, chaplygin gas, tachyon models, holographic DE models and so on [9–18]. But the origin and nature of DE still remains unknown despite many years of research and remains an open problem.

In the very recent years, cosmological studies have evidenced an additional open problem, namely the H_0 tension which arises as a result of discrepancies in the inferred value of H_0 from different types of measurements. The CMB Planck collaboration [19] (including BAO [20,21], BBN [22] and DES [23–25]) have estimated the present value of the Hubble parameter to be $H_0 \sim (67.0 - 68.5)$ km/s/Mpc. On the other hand, cosmic distance ladder and time delay measurements reported by SH0ES [26] and H0LiCOW [27] collaborations have estimated $H_0 = (74.03 \pm 1.42)$ km/s/Mpc which has been obtained from the Hubble Space Telescope observations of 70 long-period Cepheids in the Large Magellanic Cloud [26]. At the beginning the origin of this discrepancy was thought to be from the systematic. Currently the discrepancy has moved to the order of $\simeq 6\sigma$ forcing us to expand our thinking beyond the ΛCDM.

There have been a number of attempts to address these problems (See [28–30] and the references therein), which includes different dynamical dark energy models with a dynamical equation of state ($w_{DE} \neq -1$) for the dark energy (DE) component [31–33]. It has already been shown by a number of authors that a phantom-like equation of state (EoS) of the dark energy sector can effectively speed up the acceleration of the universe which results in a higher value of the Hubble parameter H_0 [34–36].

There have been a number of attempts to address these problems (See [28–30] and the references therein), which includes different dynamical dark energy models with a dynamical equation of state ($w_{DE} \neq -1$) for the dark energy (DE) component [31–33]. Modification of the dark energy sector both in the early times and late times have been proposed as the solutions to

* Corresponding author.
E-mail addresses: nandan.roy@mahidol.ac.th (N. Roy), vbsangita91@gmail.com (S. Goswami), sudipta.das@visva-bharati.ac.in (S. Das).

https://doi.org/10.1016/j.dark.2022.101037
2212-6864/

the H_0 tension. Though several works [37–39] have suggested that the early time modifications work better than the late time modifications, a modification of both the early time and late time physics might be needed to fully solve the H_0 tension [39]. In late time modification of the dark energy sector, it has been also reported that phantom models perform better than quintessence models when one considers the H_0 tension. Even the quintessence models make the H_0 tension worse [40]. In [41] it has been shown that if one considers the late time modification as a small perturbative deviation from the ΛCDM, the necessary condition to solve the H_0 tension would be phantom-like EoS of the dark energy. This is because a phantom-like equation of state (EoS) of the dark energy sector can effectively speed up the acceleration of the universe which results in a higher value of the Hubble parameter H_0 [34–36].

Since there is no preferred theoretical model of dark energy (DE) which can perfectly describe all the observed phenomena of the late time dynamics of the universe, there have been attempts to construct theoretical models of DE right from the observational data. A very useful approach in this context is parametrization of DE models in which a functional form of a particular DE parameter, viz, equation of state (EoS) of the dark energy, Hubble parameter etc. is chosen. Then the evolutions of the cosmological parameters are studied and various cosmological data sets are used to constrain these parameters.

In this work, we revisited the quintessence and phantom scalar field models and present a general scheme to write down the relevant cosmological parameters in terms of the normalized Hubble parameter $E(z) = H(z)/H_0$, current matter density Ω_{m0} and the redshift z. The interesting aspect of this approach is that the final expressions of the cosmological parameters do not explicitly depend on the nature of the scalar field. We have considered a parametrization of the Hubble parameter $H(z)$, which is one of the most crucial and important parameter for understanding the evolution of the universe. One can, in principle, parametrize the dark energy equation of state (EoS) w_{DE} or the dark energy density ρ_{DE} as well; but the contributions from the dark energy sector eventually enter the dynamics through the evolution of $H(z)$. This is one of the reasons why we chose to parametrize $H(z)$, as all other cosmological parameters are directly related to it. Till now a number of parametric forms of Hubble parameter have been proposed (see [42–44] and the references therein) in the context of quintessence scalar field models of DE.

We have considered a general approach in which the field equations have been written in terms of the switch parameter ϵ which can represent both the quintessence ($\epsilon = +1$) as well as phantom scalar field models ($\epsilon = -1$). A publicly available version of the Boltzmann code CLASS [45–47] has been amended to study the numerical evolution of the model. A detailed cosmological data analysis has been done using the MCMC code Montepython V3.5 [48,49] using various cosmological data sets. We have also compared our model which we name ϕCDM hereafter with the Λ Cold Dark Matter (ΛCDM) model using the concept of Bayes factor.

The present paper is arranged as follows. The basic mathematical formulation and the dynamics of the scalar field have been presented in Section 2. This section also deals with the parametrization of $E(z)$ and derivation of analytical expressions for various cosmological parameters corresponding to this parametrization. The observational constraints on the parameters of the model and the numerical evolution of the cosmological system have been summarized in Sections 3.1 and 3.2 respectively. Finally we conclude by presenting our results and findings in Section 4.

2. Scalar field dynamics

For a spatially flat, homogeneous and isotropic FRW universe filled with the scalar field, the Einstein's field equations and KG equation for the scalar field are given by (with $8\pi G = c = 1$)

$$3H^2 = \rho_m + \rho_\phi = \rho_m + \frac{1}{2}\epsilon\dot{\phi}^2 + V(\phi), \tag{1}$$

$$2\dot{H} + 3H^2 = -p_\phi = -\frac{1}{2}\epsilon\dot{\phi}^2 + V(\phi), \tag{2}$$

$$\epsilon\ddot{\phi} + 3\epsilon H\dot{\phi} + \frac{dV}{d\phi} = 0, \tag{3}$$

where $H = \frac{\dot{a}}{a}$ is the Hubble parameter, ρ_m is the matter energy density. The index ϵ, which is named as the switch parameter, characterizes the nature of the scalar field ϕ. If $\epsilon = +1$ the field is quintessence field and if $\epsilon = -1$ the field is phantom in nature.

The matter energy density is represented by ρ_m, which varies with the scale factor as $\rho_m = \rho_{m0}a^{-3}$ where ρ_{m0} is the current value of the matter energy density. The energy density for the scalar field can be expressed as $\rho_\phi = \frac{1}{2}\epsilon\dot{\phi}^2 + V(\phi)$ and the pressure component as $p_\phi = \frac{1}{2}\epsilon\dot{\phi}^2 - V(\phi)$. $V(\phi)$ is the potential associated with the scalar field ϕ.

By simple rearrangement of terms, from Eqs. (1), (2) and (3) it is possible to express the derivative of the Hubble parameter ($\dot{H}$) and scalar field potential $V(\phi)$ as,

$$2\dot{H} = -\frac{\rho_{m0}}{a^3} - \epsilon\dot{\phi}^2 \tag{4}$$

and

$$V(\phi) = \dot{H} + 3H^2 - \frac{\rho_{m0}}{2a^3} \tag{5}$$

A further rearrangement of Eq. (4) and use of the standard relation $\dot{H} = \frac{1}{2}a\frac{d}{da}(H^2)$ gives

$$a\frac{d}{da}(H^2) + \frac{\rho_{m0}}{a^3} = -\epsilon\dot{\phi}^2. \tag{6}$$

Again $\dot{\phi}$ can be expressed as

$$\dot{\phi} = aH\left(\frac{d\phi}{da}\right). \tag{7}$$

Using Eqs. (6) and (7), the derivative of the scalar field ϕ with respect to redshift z can be expressed as

$$\frac{d\phi}{dz} = \left[\frac{2E\frac{dE}{dz} - 3\Omega_{m0}(1+z)^2}{\epsilon E^2(1+z)}\right]^{\frac{1}{2}} \tag{8}$$

Here, we introduce the normalized Hubble parameter $E(z) = \frac{H(z)}{H_0}$, where H_0 is the present value of Hubble parameter and $\Omega_{m0} = \frac{\rho_{m0}}{3H_0^2}$ corresponds to the present value of the matter density parameter. From now onwards, in the text we would denote $E(z)$ by simply E for the convenience of writing the equations.

In a similar fashion it is possible to express the scalar field potential given in Eq. (5) in terms of $E(z)$, Ω_{m0}, and z as

$$\frac{V(z)}{3H_0^2} = -\frac{(1+z)}{3}E\frac{dE}{dz} + E^2 - \frac{1}{2}\Omega_{m0}(1+z)^3 \tag{9}$$

One can consider $\frac{V(z)}{3H_0^2}$ as the effective potential for the scalar field (in units of critical density $\rho_{crit} = 3H_0^2$ since $8\pi G = 1$). It is interesting to note that in the expressions of $V(\phi)$ or equivalently $V(z)$ given in Eqs. (5) or (9), there is no explicit dependency on the switch parameter ϵ. This behavior is expected as the nature of a scalar field depends on the kinetic term and not on the potential term.

It is also possible to express the density parameter for the matter field (Ω_m), density parameter for the scalar field (Ω_ϕ), the equation of state parameter ($w_\phi(z)$) and the deceleration parameter $q(z)$ in terms of the normalized Hubble parameter $E(z)$ as

$$\Omega_m(z) = \frac{\rho_m}{3H^2} = \frac{\Omega_{m0}(1+z)^3}{E^2}, \tag{10}$$

$$\Omega_\phi(z) = 1 - \Omega_m(z) = 1 - \frac{\Omega_{m0}(1+z)^3}{E^2}, \tag{11}$$

$$w_\phi(z) = \frac{-1 - \frac{2\dot{H}}{3H^2}}{\Omega_\phi} = \frac{\frac{2}{3}(1+z)E\frac{dE}{dz} - E^2}{E^2 - \Omega_{m0}(1+z)^3}, \tag{12}$$

$$q(z) = -1 - \frac{\dot{H}}{H^2} = \frac{(1+z)}{E}\frac{dE}{dz} - 1. \tag{13}$$

Similar to the potential $V(\phi)$, for the above set of Eqs. (10) to (13) also, it is evident that all the relevant cosmological parameters are independent of the switch parameter ϵ and hence are identical for quintessence as well as phantom fields. However, it deserves mention here that this independence is only apparent and the inherent dependency on ϵ comes through the evolution of the normalized Hubble parameter $E(z)$. Since the evolution of $E(z)$ directly depends on the nature of the scalar field, i.e, on the value of ϵ, the evolution history will obviously be different for quintessence and phantom fields even if we consider the same form of potential for both. One very important aspect to note here is that in Eq. (8), for the term $\frac{d\phi}{dz}$ to be real, two different conditions needs to be satisfied. For the quintessence field $2E\frac{dE}{dz} - 3\Omega_{m0}(1+z)^2 > 0$ and for the phantom field $2E\frac{dE}{dz} - 3\Omega_{m0}(1+z)^2 < 0$. More interestingly the dark energy EoS given in Eq. (12) can be recast as

$$w_\phi(z) = -1 + \frac{1+z}{3\Omega_\phi E^2}\left(2E\frac{dE}{dz} - 3\Omega_{m0}(1+z)^2\right), \tag{14}$$

which is directly related to the nature of the scalar field as mentioned above. As long as the quantity $2E\frac{dE}{dz} - 3\Omega_{m0}(1+z)^2$ is positive, the scalar field will behave as a quintessence field. Eventually as the scalar field evolves with time and the quantity $2E\frac{dE}{dz} - 3\Omega_{m0}(1+z)^2$ becomes negative, the field will behave as a phantom one. The phantom crossing will occur at a redshift $z = z_\lambda$ for which $2E\frac{dE}{dz} - 3\Omega_{m0}(1+z)^2 = 0$ and the EoS of the scalar field will coincide with that for the cosmological constant. A general conclusion regarding the phantom barrier crossing for the DE models can be drawn from here. Any dark energy model for which $2E\frac{dE}{dz} - 3\Omega_{m0}(1+z)^2 > 0$ for $z > z_\lambda$, and $2E\frac{dE}{dz} - 3\Omega_{m0}(1+z)^2 < 0$ for $z < z_\lambda$ should undergo a phantom barrier crossing.

Conventionally one can consider a particular form of a potential $V(\phi)$ and study the evolution of the quintessence field and phantom field separately. In our current approach one can consider a particular parametrization of $E(z)$ and reconstruct all the cosmological parameters from it. Though consideration of a particular form of $E(z)$ is equivalent to the consideration of a potential in view of Eq. (9), the advantage of our approach is that one can study both the quintessence and phantom field in a single framework. Moreover recent cosmological data sets can be used to constrain the cosmological parameters together with the EoS of the dark energy which can also help us to determine the nature of the scalar field, quintessence or phantom.

In the present work we have considered the following parametrization of the normalized Hubble parameter $E(z)$ as toy model, in order to reconstruct other cosmological parameters,

$$E(z) = \left[1 + pz\left(b + \frac{z}{c} + \frac{z^2}{d}\right)\right]^{\frac{1}{2}} \tag{15}$$

where b, c, d and p are nonzero real numbers. We have put c and d in the denominator, so as to make it sure that c, d are nonzero parameters and the polynomial parametrization considered is nonlinear for all values of c and d. Also this will ensure that even if when $p = 0$, the parametrization will not lead to any unphysical result. Now the Hubble parameter $H(z)$ can be expressed as,

$$H^2(z) = {H_0}^2\left[1 + pz\left(b + \frac{z}{c} + \frac{z^2}{d}\right)\right]. \tag{16}$$

The functional form chosen in Eq. (15) (or equivalently in Eq. (16)) is completely phenomenological, where $H^2(z)$ happens to be a second order polynomial in z. Also it can be seen from Eq. (15) that at $z = 0$, $H(z) = H_0$ and one gets back the present value of the Hubble parameter. Notice that for the choice of $p = 0$, the above equation also represents the current value of the Hubble parameter, thus the second term in the above parametrization can be considered as the deviation from the present value of the normalized Hubble parameter. For non zero values of the parameter p, at late times when $z \ll 1$, the deviation is small but for early times, when $z > 1$, it can have large deviation depending on the choice of the parameters. This behavior is expected for any parameterized quantity from the observational point of view.

Now for this particular choice of $E(z)$ given by (15), Eqs. (10), (11), (12) and (13) take the form

$$\Omega_m(z) = \frac{\Omega_{m0}(1+z)^3}{\left[1 + pz\left(b + \frac{z}{c} + \frac{z^2}{d}\right)\right]} \tag{17}$$

$$\Omega_\phi(z) = 1 - \frac{\Omega_{m0}(1+z)^3}{\left[1 + pz\left(b + \frac{z}{c} + \frac{z^2}{d}\right)\right]} \tag{18}$$

$$w_\phi(z) = \frac{p\left(b - 2bz + \frac{2z}{c} - \frac{z^2}{c} + \frac{3z^2}{d}\right) - 3}{3\left[1 + pz\left(b + \frac{z}{c} + \frac{z^2}{d}\right) - \Omega_{m0}(1+z)^3\right]} \tag{19}$$

and

$$q(z) = \frac{p\left(b - bz + \frac{2z}{c} + \frac{3z^2}{d} + \frac{z^3}{d}\right) - 2}{2\left[1 + pz\left(b + \frac{z}{c} + \frac{z^2}{d}\right)\right]} \tag{20}$$

For the sake of completeness, using Eq. (15) in Eqs. (8) and (9), we have also provided the expressions for the potential $\phi(z)$ and $V(\phi)$ for this particular choice of $E(z)$.

$$\phi(z) = \int\left[\frac{p\left(b + \frac{2z}{c} + \frac{3z^2}{d}\right) - 3\Omega_{m0}(1+z)^2}{\epsilon(1+z)\left[1 + pz\left(b + \frac{z}{c} + \frac{z^2}{d}\right)\right]}\right]^{\frac{1}{2}} dz \tag{21}$$

and

$$\frac{V(z)}{3H_0^2} = -\frac{p(1+z)\left(b + \frac{2z}{c} + \frac{3z^2}{d}\right)}{6} + \left[1 + pz\left(b + \frac{z}{c} + \frac{z^2}{d}\right)\right] - \frac{1}{2}\Omega_{m0}(1+z)^3 \tag{22}$$

The expression for the scalar field EoS w_ϕ, given in Eq. (19), can be equivalently written in a more compact form in terms of the scale factor $(\frac{a}{a_0})$ as

$$w_\phi = \frac{3w_0\left(\frac{a}{a_0}\right)^3 + 2w_1\left(\frac{a}{a_0}\right)^2 + w_3\left(\frac{a}{a_0}\right)}{3\left[w_2 - w_0\left(\frac{a}{a_0}\right)^3 - w_1\left(\frac{a}{a_0}\right)^2 - w_3\left(\frac{a}{a_0}\right)\right]}, \tag{23}$$

where w_0, w_1, w_2, w_3 are new set of parameters which are related to our old set of parameters p, b, c, d in the following way:

$$w_0 = [p(bcd - d + c) - cd], \quad w_1 = p[2d - bcd - 3c],$$

$$w_3 = p(3c - d) \text{ and } w_2 = pc - \Omega_{m0}cd\ .$$

All others cosmological parameters can also be written in terms of the new set of parameters w_0, w_1, w_2, w_3 (please see Appendix A for details). From Eq. (23), the present value of the EoS of the dark energy $w_{\phi 0}$ can be expressed as

$$w_{\phi 0} = -1 + \delta(w_0, w_1, w_2, w_3),$$

where $\delta(w_0, w_1, w_3) = \frac{w_1 - 3w_2 + 2w_3}{3(w_0 + w_1 + w_3 - w_2)}$ can be considered as the deviation from the pure ΛCDM model at present. One can recover ΛCDM model ($w_{\phi 0} = -1$) when $w_1 - 3w_2 + 2w_3 = 0$ or equivalently $pb = 3\Omega_{m0}$ at present. Hence, depending on the values of the model parameters (w_0, w_1, w_2, w_3) or equivalently (b, c, d, p and Ω_{m0}), the present value of the EoS will be either in the quintessence region or in the phantom region.

This general setup gives us the advantage to study both the quintessence and phantom field together. It would be interesting to investigate the dynamics of the dark energy sector considering the above mentioned parametrization of the EOS of the dark energy, or equivalently the scalar field models, against the current cosmological data.

3. Numerical investigation and observational constraint

Our aim here is to study the numerical evolution of our model and find the observational constraints on the cosmological parameters by comparing it to the observational data sets. In order to do so we have used the expression of w_ϕ given in Eq. (23) and amended a public version of the CLASS Boltzmann code to include it in the dark energy sector as a fluid. From now onward, we will name this scalar field model as ϕCDM model. It has been shown in [50,51] that the same late time dynamics of the scalar field dark energy models can be achieved for a variety of potentials. The late time dynamics is governed by the EoS parameter of the scalar field and similar forms of EoS parameter can be obtained for a large class of potentials. Thus it is expected that, consideration of the EoS of the scalar field as a fluid in the CLASS code will resemble the same dynamics as the scalar field itself. In Appendix B, we have presented a comparison between the analytical solutions for different cosmological parameters obtained in this work and the corresponding numerical solutions obtained from CLASS code. The MCMC code Montepython3.5 [48] has been used to estimate the relevant cosmological parameters.

3.1. Observational constraints

Cosmological data sets which we have used for the analysis are as follows: Pantheon [52], BAO (BOSS DR12 [53], 6dFGS [54], eBOSS DR14 (Lya) [55] and WiggleZ [56]). We have also included (SDSS LRG DR7 [57], SDSS LRG DR4 [58] and WiggleZ [56]) which are the observations related to cluster counts. A SH0ES prior together with the compressed Planck likelihood has been imposed. The compressed Planck likelihood has more or less the same constraining ability as the full Planck likelihood. It has been constructed by considering only three parameters, the baryon physical density $\omega_b = \Omega_b h^2$ and the two shift parameters $\theta_* = r_s(z_{dec})/D_A(z_{dec})$ and $\mathcal{R} = \sqrt{\Omega_M H_0^2} D_A(z_{dec})$, where z_{dec} is the redshift at decoupling and D_A is the comoving angular diameter distance. For more details on the compressed Planck likelihood please see Appendix A of [59].

We have made the choice of flat priors on the base cosmological parameters as follows: the baryon density $100\omega_b = [1.9, 2.5]$; cold dark matter density $\omega_{cdm} = [0.095, 0.145]$; Hubble parameter $H_0 = [60, 80]$ km s^{-1} Mpc^{-1}.

A wide range of flat prior on the model parameters w_0, w_1, w_3: $w_0 = [0, 300]$, $w_1 = [-50, 50]$ and $w_3 = [-50, 50]$ has been considered. We have fixed the model parameter w_2 to be zero. This choice has been considered from the point of view of the stability of the CLASS code and also to minimize the shooting failure. The choice of $w_2 = c(p - \Omega_{m0}\, d) = 0$ establishes a relation between p, Ω_{m0} and d as $\Omega_{m0} = \frac{p}{d}$, which does not put any tight constraint on other model parameters w_0, w_1 and w_3; there will be always room for suitable choice of parameters which can lead to a viable cosmological model.

In Fig. 1, we have shown the triangular plot which shows the 2D and 1D posterior distribution of the cosmological parameters $100w_b$, w_{cdm}, H_0, Ω_m and σ_8. A comparison has been made with the ΛCDM case represented by red plots in the figure. The constraints on the various cosmological parameters for the ΛCDM and the ϕCDM models have been enlisted in Table 1. Although there is a slight increment in the value of H_0 for the ϕCDM model, but it is far from solving the Hubble tension. A similar result of slight increment of the H_0 parameter from ΛCDM value for the scalar field models has been reported in [60,61]. Both these works analyze a large class of potentials for scalar field models and reported its inability to solve the H_0 tension.

The observational constraints on the model parameters including the dark energy EoS are shown in Fig. 2. The best fit value of the EoS of the dark energy is found to be $w_{DE} = -1.04^{+0.0204}_{-0.0166}$ which is in the phantom region. In Fig. 3, we have plotted the posterior probability $Pr(w|z)$ of the dark energy EOS w_ϕ against z. The deeper blue region enclosed by the solid lines represents $1\sigma(68\%)$ contour level and the lighter blue region represents $2\sigma(95\%)$ contour level. This plot suggests a phantom crossing of the universe around $z = 2.7$ which occurs following the conditions mentioned in Section 2.

In Fig. 4, we have shown the posterior probability of the expansion rate of the universe $H(z)/(1+z)$ with respect to z. For comparison we have plotted the observational data from Sh0ES [62] and BAO observations [63–66]. The blue line corresponds to the ϕCDM model and the red line corresponds to the ΛCDM model. The deeper and lighter blue and green regions represent the $1\sigma(68\%)$ and $2\sigma(95\%)$ contour level for the ϕCDM and ΛCDM model respectively. A similar plot for the posterior probability of the deceleration parameter $q(z)$ is given in Fig. 5 with 1σ and 2σ confidence level. A flip in the signature of the deceleration parameter is observed which indicates a transition from the decelerated phase to an accelerated phase which is a must for the unhindered structure formation of the universe.

To compare the ΛCDM model and our proposed ϕCDM model, we have used χ^2_{min} value difference between the models, $\Delta\chi^2_{min} = \chi^2_\phi - \chi^2_\Lambda = -5$ (see Table 1). This indicates that the proposed ϕCDM model gives a better fit to the data as compared to the ΛCDM model. We have also computed the Bayesian evidence for model selection to be more certain about the preference on the model from data. Bayes factor is used to penalize the complex models involving many parameters and hence to avoid overfitting. To compare the models we have computed $\ln B_{\phi\Lambda} = \ln \mathcal{Z}_\phi - \ln \mathcal{Z}_\Lambda$, where $\mathcal{Z}$ is the Bayesian evidence. According to Jeffreys' scale, the strength of preference on ϕCDM over ΛCDM will depend on the value of $\ln B_{\phi\Lambda}$. If $\ln B_{\phi\Lambda} < 1$, the preference is negative and if $\ln B_{\phi\Lambda} > 1; > 2.5; > 5.0$ the preference is positive, moderate and strong respectively. For more details, one can refer to [67]. The calculation of the Bayes factor is numerically challenging; for this, we have used the publicly available code MCEvidence [68] which can calculate the Bayes factor directly

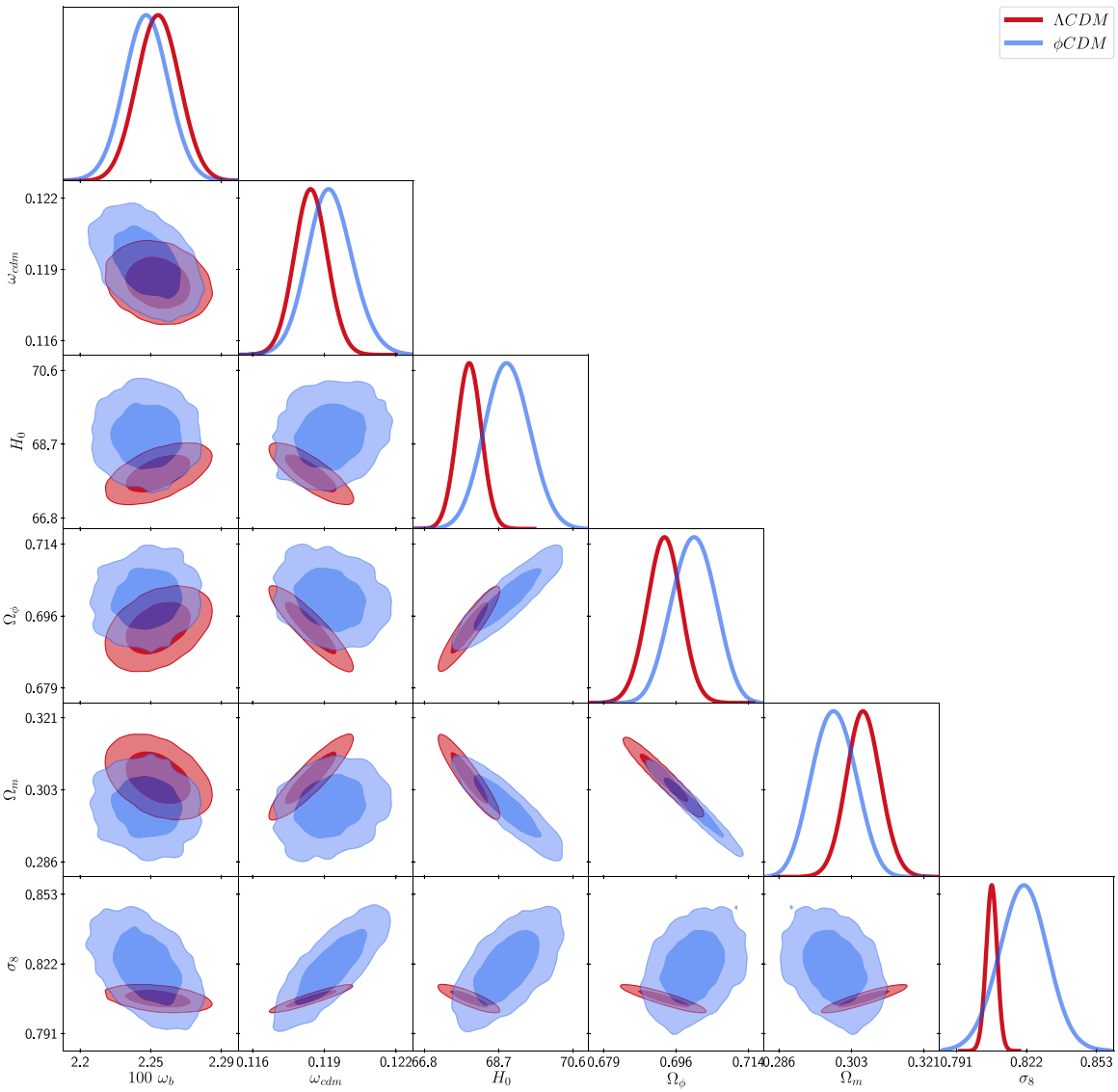

Fig. 1. Triangular plot of 2D and 1D posterior distribution of the cosmological parameters $100w_1$, w_{cdm}, H_0, Ω_m and σ_8 using various dataset mentioned in Section 3.1. (For interpretation of the references to color in this figure legend, the reader is referred to the web version of this article.)

from the MCMC chains generated by the MONTE PYTHON. As listed in Table 1, we have obtained $\ln B_{\phi\Lambda} = +2.005$ which indicates positive preference on the ϕCDM model compared to the ΛCDM model.

3.2. Numerical evolution

We have considered the observational constraints obtained on the parameters w_0, w_1, w_3 in the previous section to investigate the numerical evolution of the system. Fig. 6 shows the evolution of the EoS parameter of the scalar field component w_ϕ with respect to redshift z. To understand the effect of the model parameters w_0, w_1, w_3 on the cosmological parameters, we consider to vary one parameter keeping others fixed to the best fit values obtained from the MCMC analysis. The black dashed lines in all the plots correspond to the best fit values of the model parameters $[w_0, w_1, w_3 : 207, -30.7, 4.25]$. In the top panel of Fig. 6, we vary w_0 while keeping the parameters w_1 and w_3 fixed to the best-fit value. In the middle and bottom panels, we vary w_1 and w_3 respectively keeping the other two parameters fixed. Our choice of parameters lies well within the posteriors obtained by the MCMC analysis in the previous section. From Fig. 6 one can see that the current value of EoS of the scalar field lies in the phantom region ($w_\phi < -1$) and the universe should have

Table 1
Best fit values of different cosmological parameters for the ΛCDM and ϕCDM models. The posteriors can be seen from the triangular plots provided in Figs. 1 and 2.

Parameter	ΛCDM	ϕCDM
$100\ \omega_b$	$2.25^{+0.013}_{-0.0129}$	$2.24^{+0.0146}_{-0.0128}$
ω_{cdm}	$0.118^{+0.00069}_{-0.000705}$	$0.119^{+0.0096}_{-0.0098}$
H_0	$68^{+0.326}_{-0.319}$	$68.9^{+0.573}_{-0.602}$
Ω_{DE}	$0.694^{+0.00426}_{-0.00406}$	$0.701^{+0.00478}_{-0.00516}$
Ω_m	$0.306^{+0.00406}_{-0.00426}$	$0.299^{+0.00516}_{-0.00478}$
σ_8	$0.807^{+0.00255}_{-0.00254}$	$0.821^{+0.011}_{-0.010}$
w_{DE}	-1	$-1.04^{+0.0204}_{-0.0166}$
w_0	–	>96.97
w_1	–	< -10.03
w_3	–	$4.25^{+1.65}_{-3.46}$
$\Delta\chi^2_{min}$	0	-5
$\ln B_{\phi\Lambda}$	0	$+2.005$

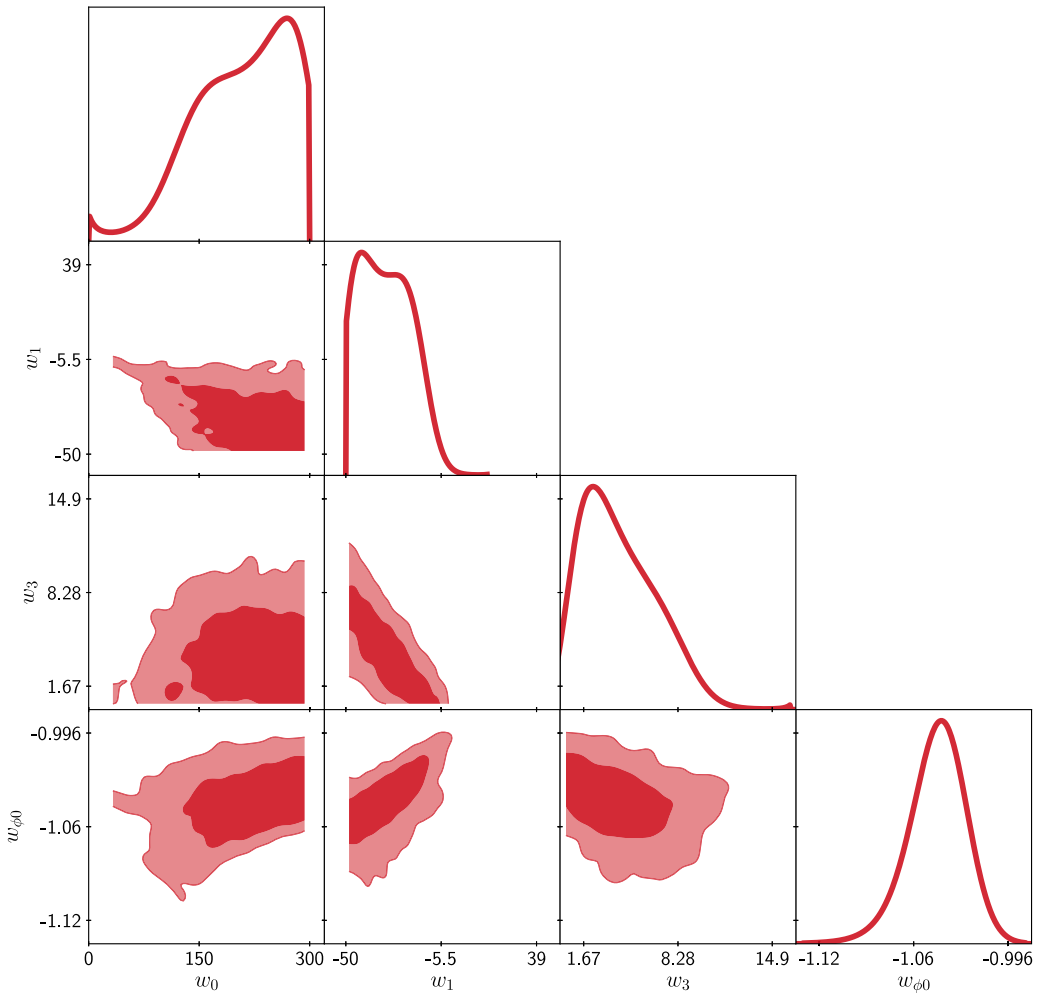

Fig. 2. Triangular plot showing observational constraints on the model parameters w_0, w_1, w_3 and the EoS of the scalar field $w_{\phi 0}$.

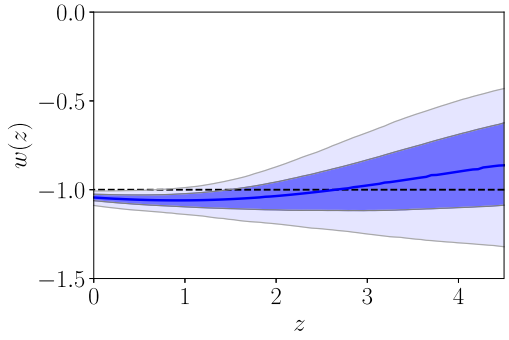

Fig. 3. This figure shows the posterior probability $Pr(w|z)$ of the dark energy EOS w_ϕ against z. The deep blue region represents $1\sigma(68\%)$ confidence contour level and the light blue regions represent the $2\sigma(95\%)$ confidence contour level. (For interpretation of the references to color in this figure legend, the reader is referred to the web version of this article.)

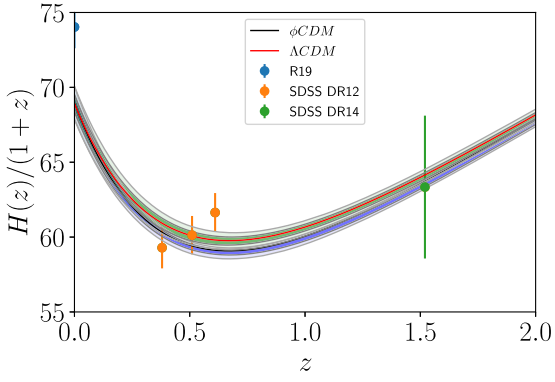

Fig. 4. The posterior probability $Pr(H|z)$ of the expansion rate of the universe $H(z)/(1+z)$ against z. The dark gray region represents $1\sigma(68\%)$ contour level and the light gray regions represent $2\sigma(95\%)$ contour level. (For interpretation of the references to color in this figure legend, the reader is referred to the web version of this article.)

undergone phantom crossing from the quintessence to phantom (see the best fit curve, black dotted line). From the top panel it is apparent that the effect of w_0 on the EoS parameter is not very significant at later epochs and also the redshift at which phantom crossing occurs is insensitive to the value of w_0. The effect of the parameter w_0 is only apparent at the early epochs of the evolution of the universe. However, the present value of the EoS parameter as well as the evolution of the EoS is quite sensitive to both the parameters w_1, w_3. This finding is in agreement with the results shown in Fig. 2 obtained by MCMC analysis. It has been observed that the evolution of the EoS parameter will be effected only when the variation of w_1 is of the order of 10 or more. The w_0, w_1 parameters appear to be unconstrained with a lower cutoff of $w_0 > 96.97$ (approximately) and a upper cutoff

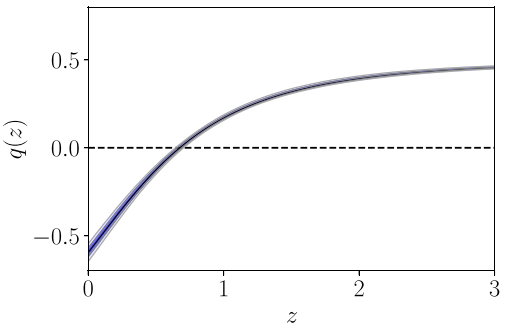

Fig. 5. This figure shows the posterior probability $Pr(q|z)$ of the deceleration parameter $q(z)$ against z. The deep blue region represents $1\sigma(68\%)$ contour level and the light blue regions represents $2\sigma(95\%)$ contour level. (For interpretation of the references to color in this figure legend, the reader is referred to the web version of this article.)

$w_1 < -5.5$ (approximately) respectively. On the other hand w_3 is tightly constrained with allowed values in the range $4.25^{+1.65}_{-3.46}$.

The evolution of the energy densities of the matter Ω_m and the scalar field Ω_ϕ components has been shown in Fig. 7. We have considered the same set of parameter values for w_0, w_1, w_3 as in Fig. 6. The blue curves represent the ΛCDM case for reference. It can be seen from the plots that the energy densities are not very sensitive to the model parameters w_0, w_1, w_3 though these parameters have significant effect on the evolution of the EoS of dark energy.

We also show in Figs. 8 and 9 the temperature anisotropies and the matter power spectrum (MPS) for the ϕCDM model corresponding to the same set of model parameters as considered in Fig. 6. For comparison, data from different experiments have been plotted as references together with the numerical solutions. For the temperature anisotropies (TT) we have used binned TT power spectrum data from Planck 18 [69]. For the MPS following data sets have been used: Planck2018 CMB data [69], SDSS galaxy clustering [70], SDSS Lyα forest [71] and DES cosmic shear data [72] (for details on full data collection, please see [73]).

The lower panels of Figs. 8 and 9 represent the relative differences in D_l and $P(k)$ in comparison to the ΛCDM case. It is observed that in case of D_l, there is notable deviation from ΛCDM case for both the lower and higher multipoles. For $P(k)$, the deviation from the ΛCDM case is observed at all scales. Although the percentage deviation is not much, but one should, in principle, take into account the dark energy perturbations as well to obtain the complete picture. A similar claim has been made in [74] that if one does not consider the dark energy perturbations, this can result in misleading constraints on the cosmological parameters. To calculate the D_l and $P(k)$ we have used the PPF (Parameterized Post-Friedmann) approximation [75] so that the dark energy perturbations can cross the phantom divider smoothly. The PPF approximation has already been implemented in the CLASS code by default.

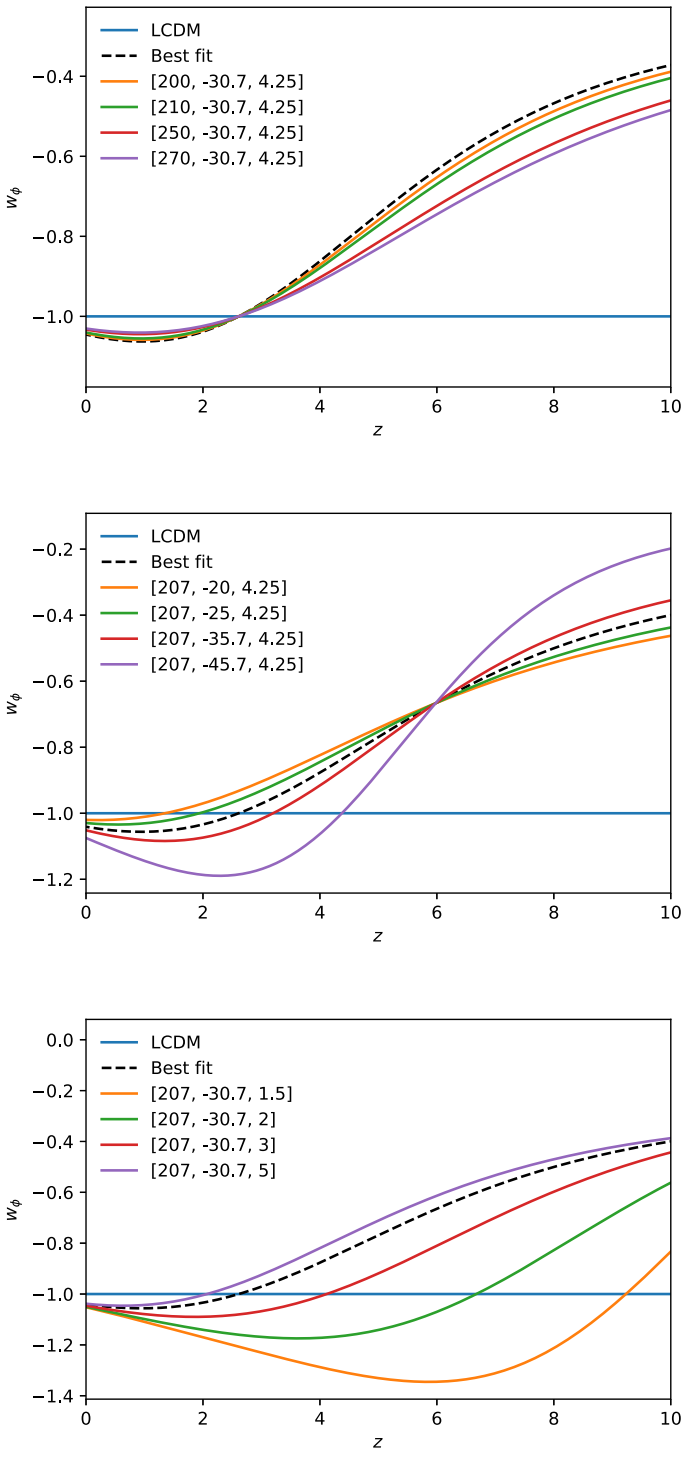

Fig. 6. The evolution of the EoS (w_ϕ) for the ϕCDM model for different choices of the model parameters (w_0, w_1, w_3) against the redshift z. The offset values refer to the respective choices of the model parameters. The solid blue line represents the ΛCDM model and the black dashed line represents the evolution of the EoS corresponding to the best fit values obtained from MCMC analysis. The top panel shows the evolution when we are varying only w_0 while keeping the parameters w_1, w_3 fixed. The middle and bottom panels show the evolution when w_1 and w_3 are evolving keeping the other two respective parameters fixed. The blue horizontal line corresponds to the ΛCDM case $w_\Lambda = -1$. (For interpretation of the references to color in this figure legend, the reader is referred to the web version of this article.)

4. Conclusion

In this work we have revisited the dynamics of the scalar field dark energy models and proposed a general scheme which can include both the quintessence and the phantom scalar field models. Our method is simple and straightforward in which it is possible to express all the cosmological parameters in terms of the redshift (z), the present value of the matter density parameter (Ω_{m0}) and the normalized Hubble parameter (E). We have obtained the expressions for various cosmological parameters and have found that the final expressions of these cosmological parameters are independent of the nature of the scalar field, either quintessence or phantom. A general condition for the phantom barrier crossing

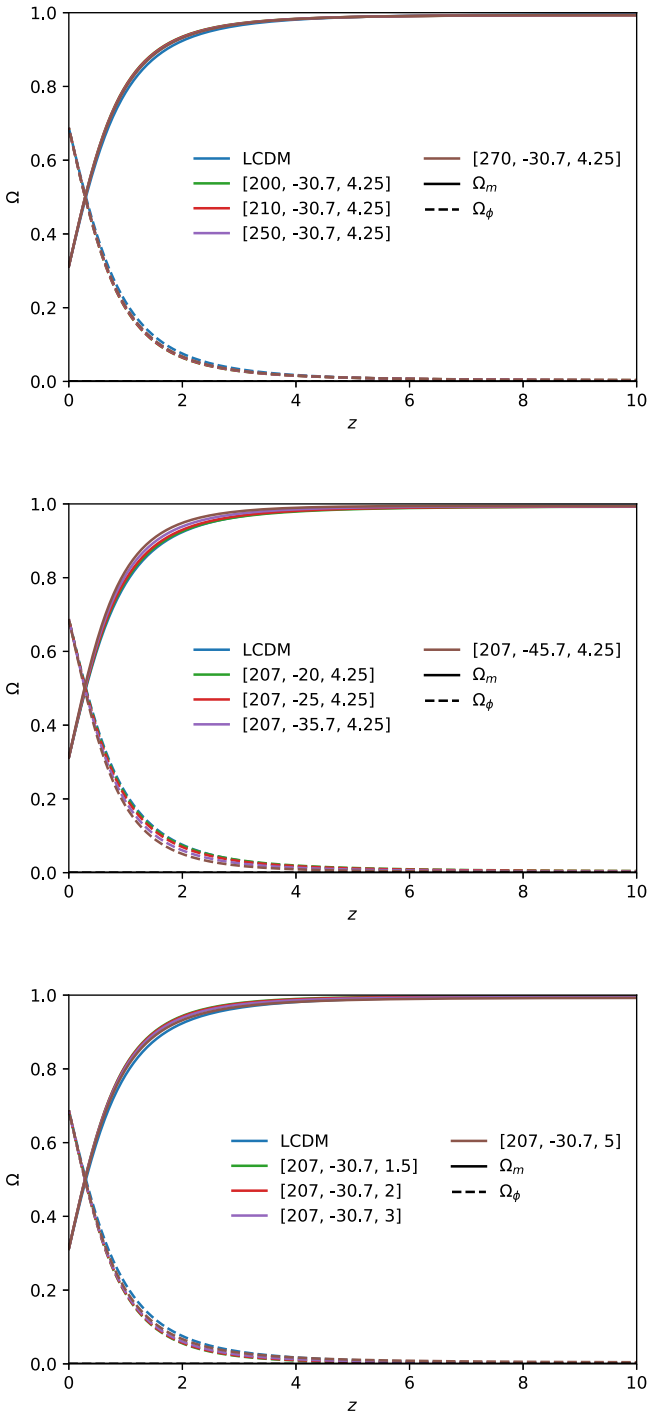

Fig. 7. The evolution of the dark energy density parameter ($\Omega_\phi(z)$) (dashed line) and the matter density parameter ($\Omega_m(z)$) (solid line). The top, middle and bottom panels correspond to the variation of the model parameters w_0, w_1 and w_3 respectively keeping other two respective model parameters fixed to the best fit values.

of the dark energy models is also obtained. This general condition is particularly interesting as it can help us to check the possibility of phantom barrier crossing for a given DE model which complies with the methodology given here without a detailed numerical study of the model. This encourages us to consider a suitable parametrization of the Hubble parameter as toy model and to study the model against the current cosmological observations.

A publicly available version of the Boltzmann code CLASS has been amended. The dynamics of the scalar field has been incorporated in the CLASS code by adding it as a fluid using our proposed parametrization. A detailed study of the model against the recent cosmological data sets has been done using the MCMC code Montepython. The best fit value of the EoS parameter for the scalar field at the current epoch comes out to be less than -1 which indicates that at present phantom DE models are preferred by observational data compared to quintessence models. However a phantom barrier crossing has been observed within 2σ confidence level for a wide range of choice of the model parameters.

The best fit value of H_0 comes out to be $68.9^{+0.573}_{-0.602}$ which happens to be more compatible with the PLANCK collaboration results and thus cannot alleviate the Hubble tension. This is in agreement with the recent results [37] where it has been shown that CMB+BAO+SN data put stronger constraints on H_0 and on other background cosmological parameters and that the addition of H_0 prior from SH0ES (or from similar other local distance observations) cannot significantly pull the H_0 value towards the corresponding SH0ES value. A comparison between ϕCDM and ΛCDM models have been carried out using the concept of Bayes Factor and the ϕCDM model is found to have positive preference over the ΛCDM one. We have also found that there are slight deviations in the D_l and $P(k)$ curves as compared to standard ΛCDM; for D_l, deviation has been observed in both lower and higher multipoles whereas for $P(k)$ the deviation has been observed at all scales.

We must admit that the choice of parametrization for $E(z)$ is motivated by mathematical simplicity and is not unique. A wide variety of parametrization can be considered which might be able to solve the H_0 tension as well. As of now, the current choice of parametrization valid for these two scalar field models can not alleviate the H_0 tension completely, but interesting results may be obtained by considering an interaction between the two dark sectors. It has been recently shown in [76] that for popular and simple choices of interaction term, the DM and DE sectors cannot exchange energy at a rate greater than 7% of the critical energy density over the course of a Hubble time which is too small to solve the coincidence problem. However a different and intricate choice of the interaction term may lead to a different result and is worth studying.

CRediT authorship contribution statement

Nandan Roy: Conceptualization, Writing – review & editing, Methodology, Software. **Sangita Goswami:** Formal analysis, Writing – original draft. **Sudipta Das:** Conceptualization, Writing – review & editing, Methodology.

Declaration of competing interest

The authors declare that they have no known competing financial interests or personal relationships that could have appeared to influence the work reported in this paper.

Acknowledgments

We are grateful to Ankan Mukherjee, Luis Urena Lopez and Francisco X. Linares Cedeño for help in the making of some plots. We acknowledge the use of the Chalawan High Performance Computing cluster, operated and maintained by the National Astronomical Research Institute of Thailand (NARIT). The research of NR is supported by Mahidol University, Thailand through the research project MU-MRC-MGR 04/2565. SD would like to acknowledge IUCAA, Pune for providing support through the associateship programme.

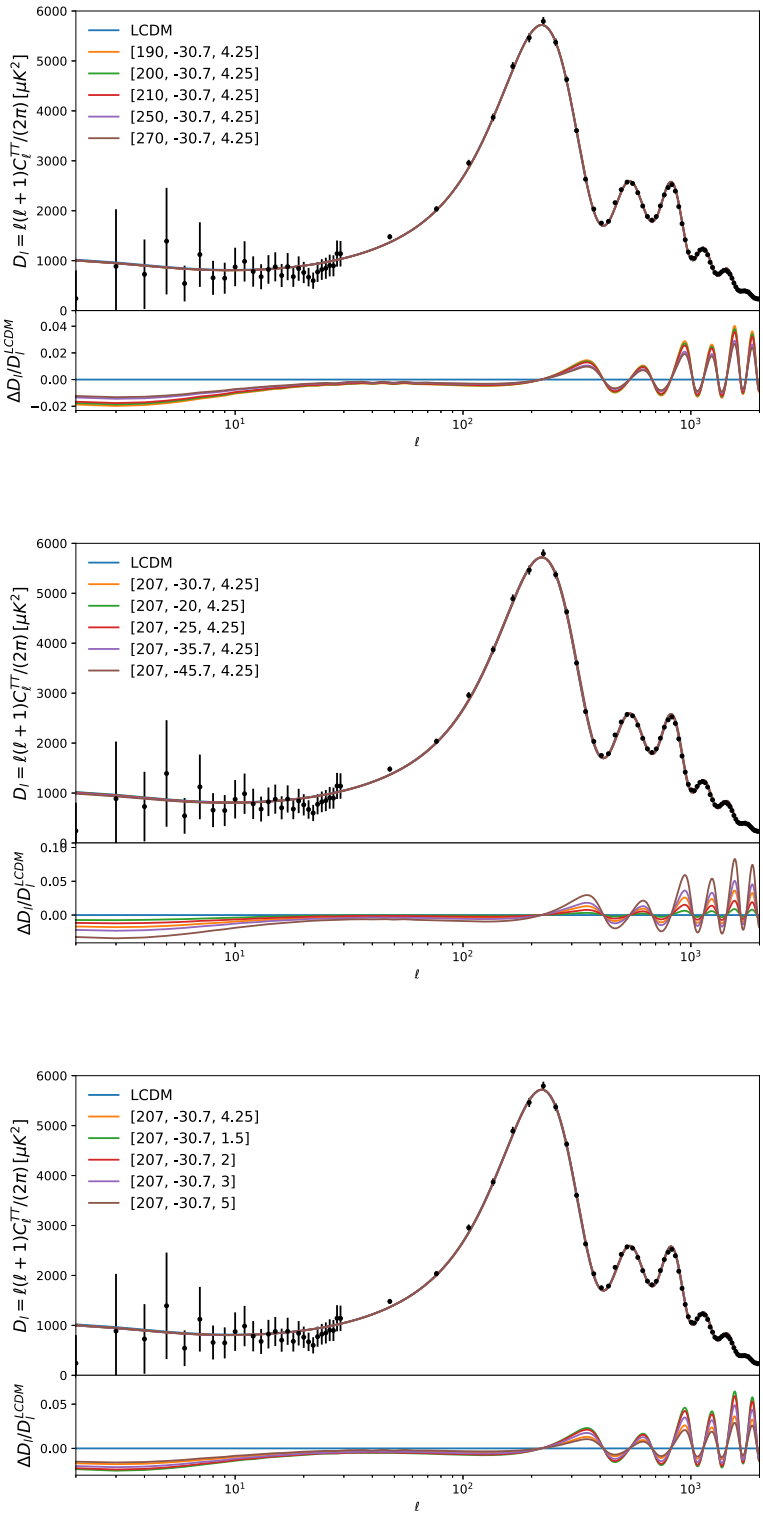

Fig. 8. Plot of the CMB anisotropies for the ϕCDM model. The top, middle and bottom panels correspond to the variation of the model parameters as explained in Fig. 6. The bottom panel of each figure shows the relative difference between the ϕCDM and the ΛCDM ($\Delta D_l = (D_l - D_l^{\Lambda CDM})/D_l^{\Lambda CDM}$).

Appendix A. Cosmological parameters in terms of w_0, w_1, w_2, w_3

In the text we have considered two different sets of parameters $[p, b, c, d]$ and $[w_0, w_1, w_2, w_3]$. Here we present all the cosmological parameters provided in Eqs. (17) to (22) in terms of the parameters w_0, w_1, w_2 and w_3.

$$E^2(z) = \frac{f_3}{f_2} \tag{A.1}$$

$$q(z) = \frac{1}{2f_3}((f_1 - w_2)(1+z)^3 + w_1(\Omega_{m0} - 1)(1+z) + 2w_0(\Omega_{m0} - 1)) \tag{A.2}$$

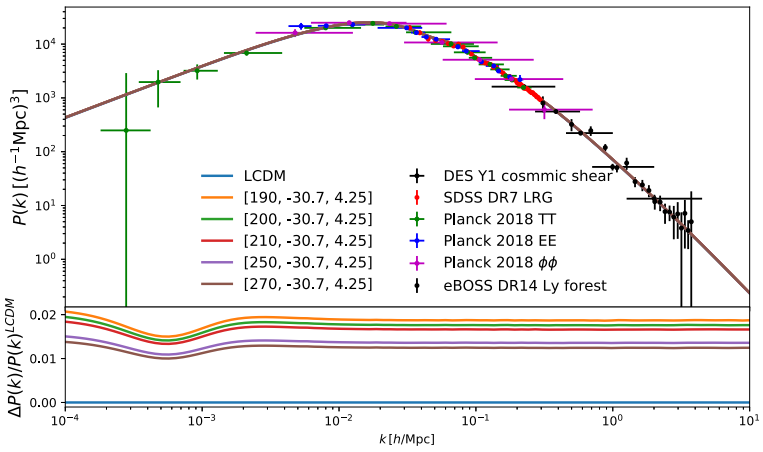

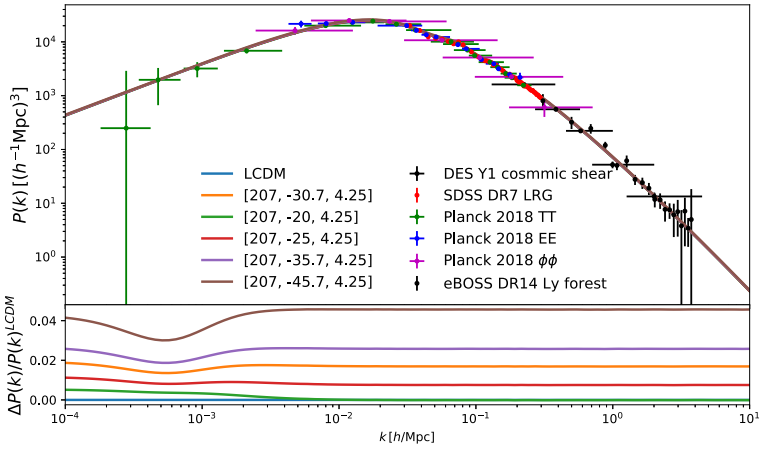

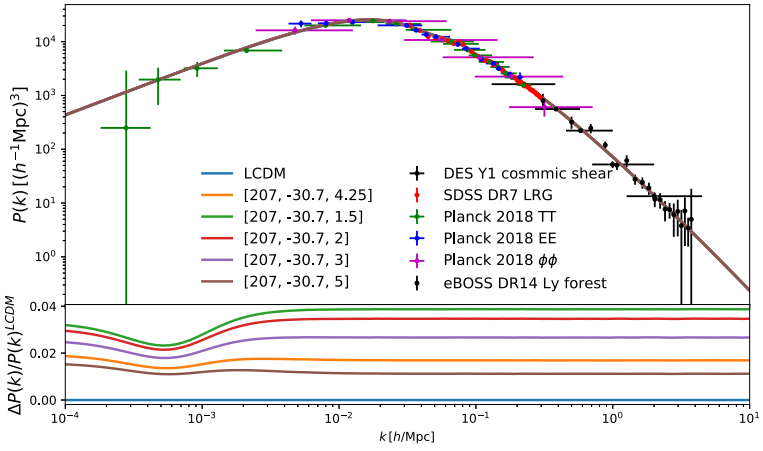

Fig. 9. Top, middle and bottom panel shows the plots of matter power spectrum (MPS) for the variation of the model parameters as explained in Fig. 6. At the bottom panel of each figure we showed relative difference between the ϕCDM and the ΛCDM models, $(\Delta P(k) = (P(k) - P(k)^{\Lambda CDM})/P(k)^{\Lambda CDM})$.

$$\Omega_m(z) = \frac{\Omega_{m0} f_2 (1+z)^3}{f_3} \tag{A.3}$$

$$\Omega_\phi = 1 - \frac{\Omega_{m0} f_2 (1+z)^3}{f_3} \tag{A.4}$$

$$\begin{aligned}\frac{V(z)}{3H_0^2} =& \frac{1}{6f_2}[-(1+z)(3(f_1 - w_2)(1+z)^2 \\ & - 2w_3(\Omega_{m0} - 1)(1+z) - w_1(\Omega_{m0} - 1)) \\ & + 6(f_1 - w_2)(1+z)^3 - 6w_3(\Omega_{m0} - 1)(1+z)^2 \\ & - 6w_1(\Omega_{m0} - 1)(1+z) - 6w_0(\Omega_{m0} - 1)] \\ & - \frac{1}{2}\Omega_{m0}(1+z)^3\end{aligned} \tag{A.5}$$

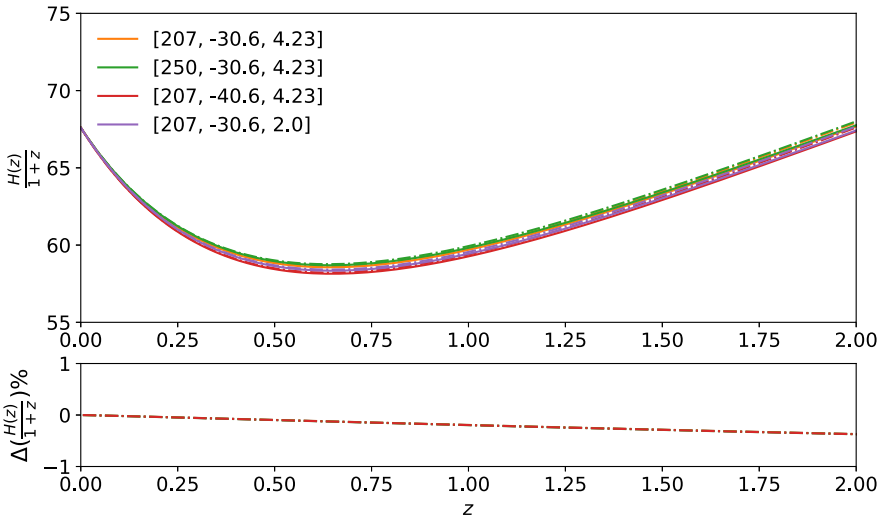

Fig. B.10. Comparison of the $H(z)/1+z$ for the numerical solutions obtained from the CLASS code (represented by solid lines) and the analytical solutions obtained from Eq. (A.1) (represented by dashed lines). In the bottom panel we have shown the percentage difference between the numerical solutions and the analytical solutions.

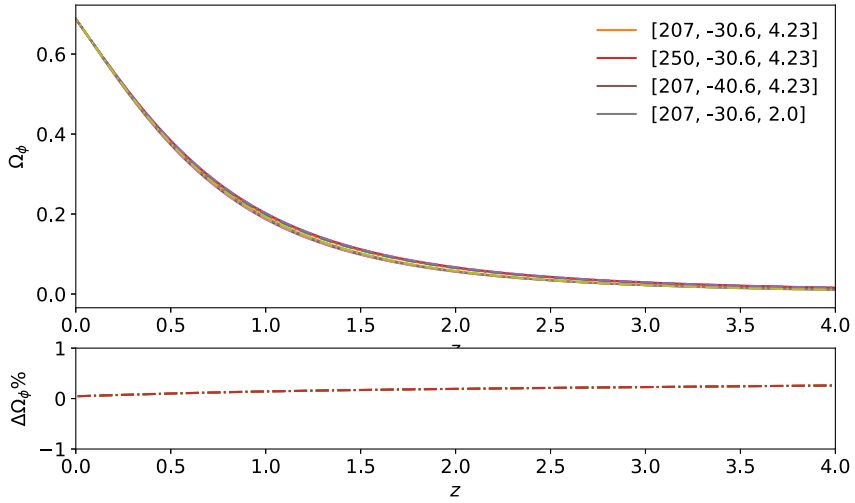

Fig. B.11. Comparison of $\Omega_\phi(z)$ for the numerical solutions obtained from the CLASS code (represented by solid lines) and the analytical solutions obtained from Eq. (A.4) (represented by dashed lines). In the bottom panel we have shown the percentage difference between the two solutions.

$$\phi(z) = \int \frac{1}{\epsilon(1+z)f_3}\Big[\big(3(f_1-w_2)(1+z)^2 - 2w_3\,(\Omega_{m0}-1)\,(1+z) - w_1\,(\Omega_{m0}-1)\big) - 3\Omega_{m0}\,f_2(1+z)^2\Big]^{1/2}\,dz \tag{A.6}$$

where

$$f_1 = (\Omega_{m0}(w_0+w_1+w_3)),$$

$$f_2 = (w_0+w_1+w_3-w_2)$$

and

$$f_3 = (f_1-w_2)(1+z)^3 - w_3(\Omega_{m0}-1)(1+z)^2 - w_1(\Omega_{m0}-1)(1+z) - w_0(\Omega_{m0}-1).$$

Appendix B. Comparison between the analytical solution and the numerical solution

In Section 3 we have mentioned that the dynamics of the scalar field has been incorporated in the CLASS code as a fluid by implementing the EoS of the DE given in Eq. (23). Here we present a comparison between the numerical solutions obtained from the CLASS code and the analytical solutions of the cosmological parameters. In Fig. B.10 we have compared the expansion rate $(H(z)/1+z)$ of the universe for these two solutions. The solid lines are the numerical solutions obtained from the CLASS code and the dashed lines are the corresponding plots for the analytical solutions which can be obtained from Eq. (A.1). The bottom panel of Fig. B.10 shows the percentage difference between the numerical and the analytical solutions. A similar comparison between the dark energy density (Ω_ϕ) parameters for the numerical and the analytical solutions has been provided in the upper panel of Fig. B.11 along with the corresponding percentage difference at the bottom panel. One can see that for both the cases the percentage difference is less than 1%. It must be mentioned here that in order to obtain the analytical solutions, we have used the Klein Gordon (KG) equation for the scalar field whereas the numerical solutions obtained from the CLASS code involve the integral of the EoS of the dark energy over redshift interval. This similarity and very little deviation justify our claim in Section 3 that if one considers the EoS of the scalar field as a fluid in the

CLASS code, it will resemble the same dynamics as that of the scalar field.

References

[1] A.G. Riess, et al., Observational evidence from supernovae for an accelerating universe and a cosmological constant, Astron. J. 116 (1998) 1009–1038, arXiv:astro-ph/9805201, doi:https://iopscience.iop.org/article/10.1086/300499.

[2] S. Perlmutter, et al., Measurements of Ω and Λ from 42 high redshift supernovae, Astrophys. J. 517 (1999) 565–586, http://dx.doi.org/10.1086/307221, arXiv:astro-ph/9812133.

[3] A. Meszaros, On the reality of the accelerating universe, Astrophys. J. 580 (2002) 12–15, http://dx.doi.org/10.1086/343071, arXiv:astro-ph/0207558.

[4] M. Arnaud, et al., Planck intermediate results. XXXI. Microwave survey of galactic supernova remnants, Astron. Astrophys. 586 (2016) A134, http://dx.doi.org/10.1051/0004-6361/201425022, arXiv:1409.5746.

[5] C.P. Ahn, R. Alexandroff, C.A. Prieto, S.F. Anderson, T. Anderton, B.H. Andrews, E. Aubourg, S. Bailey, E. Balbinot, R. Barnes, et al., The ninth data release of the sloan digital sky survey: first spectroscopic data from the SDSS-III baryon oscillation spectroscopic survey, Astrophys. J. Suppl. Ser. 203 (2) (2012) 21.

[6] A.G. Riess, P.E. Nugent, R.L. Gilliland, B.P. Schmidt, J. Tonry, M. Dickinson, R.I. Thompson, T. Budavari, S. Casertano, A.S. Evans, et al., The farthest known supernova: Support for an accelerating universe and a glimpse of the epoch of deceleration, Astrophys. J. 560 (1) (2001) 49–71, http://dx.doi.org/10.1086/322348.

[7] L. Amendola, Acceleration at z > 1? Mon. Not. R. Astron. Soc. 342 (1) (2003) 221–226, http://dx.doi.org/10.1046/j.1365-8711.2003.06540.x.

[8] T. Padmanabhan, Dark energy: mystery of the millennium, in: AIP Conference Proceedings, Vol. 861, American Institute of Physics, 2006 pp. 179–196.

[9] V. Sahni, A. Starobinsky, Reconstructing dark energy, Internat. J. Modern Phys. D 15 (12) (2006) 2105–2132.

[10] K. Bamba, S. Capozziello, S. Nojiri, S.D. Odintsov, Dark energy cosmology: the equivalent description via different theoretical models and cosmography tests, Astrophys. Space Sci. 342 (1) (2012) 155–228.

[11] C. Armendariz-Picon, V. Mukhanov, P.J. Steinhardt, Essentials of k-essence, Phys. Rev. D 63 (10) (2001) 103510.

[12] R.R. Caldwell, A phantom menace? Cosmological consequences of a dark energy component with super-negative equation of state, Phys. Lett. B 545 (1–2) (2002) 23–29.

[13] S.M. Carroll, M. Hoffman, M. Trodden, Can the dark energy equation-of-state parameter w be less than- 1? Phys. Rev. D 68 (2) (2003) 023509.

[14] A. Kamenshchik, U. Moschella, V. Pasquier, An alternative to quintessence, Phys. Lett. B 511 (2–4) (2001) 265–268.

[15] A. Sen, Tachyon matter, J. High Energy Phys. 2002 (07) (2002) 065.

[16] T. Padmanabhan, Accelerated expansion of the universe driven by tachyonic matter, Phys. Rev. D 66 (2) (2002) 021301.

[17] E.J. Copeland, M. Sami, S. Tsujikawa, Dynamics of dark energy, Internat. J. Modern Phys. D 15 (11) (2006) 1753–1935.

[18] L. Amendola, S. Tsujikawa, Dark Energy: Theory and Observations, Cambridge University Press, 2010.

[19] N. Aghanim, et al., Planck 2018 results. VI. Cosmological parameters, Astron. Astrophys. 641 (2020) A6, http://dx.doi.org/10.1051/0004-6361/201833910, arXiv:1807.06209, Erratum:; Astron. Astrophys. 652 (2021) C4.

[20] S. Alam, M. Ata, S. Bailey, F. Beutler, D. Bizyaev, J.A. Blazek, A.S. Bolton, J.R. Brownstein, A. Burden, C.-H. Chuang, et al., The clustering of galaxies in the completed SDSS-III baryon oscillation spectroscopic survey: cosmological analysis of the DR12 galaxy sample, Mon. Not. R. Astron. Soc. 470 (3) (2017) 2617–2652, http://dx.doi.org/10.1093/mnras/stx721.

[21] F. Beutler, C. Blake, M. Colless, D.H. Jones, L. Staveley-Smith, L. Campbell, Q. Parker, W. Saunders, F. Watson, The 6df galaxy survey: baryon acoustic oscillations and the local hubble constant, Mon. Not. R. Astron. Soc. 416 (4) (2011) 3017–3032, http://dx.doi.org/10.1111/j.1365-2966.2011.19250.x.

[22] S. Alam, M. Aubert, S. Avila, C. Balland, J.E. Bautista, M.A. Bershady, D. Bizyaev, M.R. Blanton, A.S. Bolton, J. Bovy, et al., Completed SDSS-IV extended baryon oscillation spectroscopic survey: Cosmological implications from two decades of spectroscopic surveys at the apache point observatory, Phys. Rev. D 103 (8) (2021) http://dx.doi.org/10.1103/physrevd.103.083533.

[23] M. Troxel, N. MacCrann, J. Zuntz, T. Eifler, E. Krause, S. Dodelson, D. Gruen, J. Blazek, O. Friedrich, S. Samuroff, et al., Dark energy survey year 1 results: Cosmological constraints from cosmic shear, Phys. Rev. D 98 (4) (2018) http://dx.doi.org/10.1103/physrevd.98.043528.

[24] T. Abbott, F. Abdalla, A. Alarcon, J. Aleksić, S. Allam, S. Allen, A. Amara, J. Annis, J. Asorey, S. Avila, et al., Dark energy survey year 1 results: Cosmological constraints from galaxy clustering and weak lensing, Phys. Rev. D 98 (4) (2018) http://dx.doi.org/10.1103/physrevd.98.043526.

[25] E. Krause, T.F. Eifler, J. Zuntz, O. Friedrich, M.A. Troxel, S. Dodelson, J. Blazek, L.F. Secco, N. MacCrann, E. Baxter, C. Chang, N. Chen, M. Crocce, J. DeRose, A. Ferte, N. Kokron, F. Lacasa, V. Miranda, Y. Omori, A. Porredon, R. Rosenfeld, S. Samuroff, M. Wang, R.H. Wechsler, T.M.C. Abbott, F.B. Abdalla, S. Allam, J. Annis, K. Bechtol, A. Benoit-Levy, G.M. Bernstein, D. Brooks, D.L. Burke, D. Capozzi, M.C. Kind, J. Carretero, C.B. D'Andrea, L.N. da Costa, C. Davis, D.L. DePoy, S. Desai, H.T. Diehl, J.P. Dietrich, A.E. Evrard, B. Flaugher, P. Fosalba, J. Frieman, J. Garcia-Bellido, E. Gaztanaga, T. Giannantonio, D. Gruen, R.A. Gruendl, J. Gschwend, G. Gutierrez, K. Honscheid, D.J. James, T. Jeltema, K. Kuehn, S. Kuhlmann, O. Lahav, M. Lima, M.A.G. Maia, M. March, J.L. Marshall, P. Martini, F. Menanteau, R. Miquel, R.C. Nichol, A.A. Plazas, A.K. Romer, E.S. Rykoff, E. Sanchez, V. Scarpine, R. Schindler, M. Schubnell, I. Sevilla-Noarbe, M. Smith, M. Soares-Santos, F. Sobreira, E. Suchyta, M.E.C. Swanson, G. Tarle, D.L. Tucker, V. Vikram, A.R. Walker, J. Weller, Dark energy survey year 1 results: Multi-probe methodology and simulated likelihood analyses, 2017, arXiv:1706.09359.

[26] A.G. Riess, S. Casertano, W. Yuan, L.M. Macri, D. Scolnic, Large magellanic cloud cepheid standards provide a 1 the determination of the hubble constant and stronger evidence for physics beyond Λ CDM, Astrophys. J. 876 (1) (2019) 85, http://dx.doi.org/10.3847/1538-4357/ab1422.

[27] K.C. Wong, S.H. Suyu, G.C.-F. Chen, C.E. Rusu, M. Millon, D. Sluse, V. Bonvin, C.D. Fassnacht, S. Taubenberger, M.W. Auger, et al., H0LiCOW – xIII. A 2.4 per cent measurement of H0 from lensed quasars: 5.3 tension between early- and late-universe probes, Mon. Not. R. Astron. Soc. 498 (1) (2019) 1420–1439, http://dx.doi.org/10.1093/mnras/stz3094.

[28] B.D. Normann, I.H. Brevik, Can the hubble tension be resolved by bulk viscosity? Modern Phys. Lett. A 36 (27) (2021) 2150198, http://dx.doi.org/10.1142/s0217732321501984.

[29] E. Di Valentino, O. Mena, S. Pan, L. Visinelli, W. Yang, A. Melchiorri, D.F. Mota, A.G. Riess, J. Silk, In the realm of the Hubble tension—a review of solutions *, Classical Quantum Gravity 38 (15) (2021) 153001, http://dx.doi.org/10.1088/1361-6382/ac086d.

[30] M. Petronikolou, S. Basilakos, E.N. Saridakis, Alleviating H_0 tension in horndeski gravity, 2021, arXiv:2110.01338.

[31] D. Benisty, D. Staicova, A preference for dynamical dark energy?, 2021, arXiv:2107.14129.

[32] T. Karwal, M. Raveri, B. Jain, J. Khoury, M. Trodden, Chameleon early dark energy and the hubble tension, 2021, arXiv:2106.13290.

[33] F.X.L. Cedeño, N. Roy, L.A. Ureña-López, Tracker phantom field and a cosmological constant: dynamics of a composite dark energy model, 2021, arXiv:2105.07103.

[34] G. Alestas, L. Kazantzidis, L. Perivolaropoulos, H0 tension, phantom dark energy, and cosmological parameter degeneracies, Phys. Rev. D 101 (12) (2020) http://dx.doi.org/10.1103/physrevd.101.123516.

[35] E. Di Valentino, A. Mukherjee, A.A. Sen, Dark energy with phantom crossing and the H0 tension, Entropy 23 (4) (2021) 404, http://dx.doi.org/10.3390/e23040404.

[36] S. Vagnozzi, New physics in light of the H0 tension: An alternative view, Phys. Rev. D 102 (2) (2020) http://dx.doi.org/10.1103/physrevd.102.023518.

[37] B.R. Dinda, Cosmic expansion parametrization: Implication for curvature and H_0 tension, Phys. Rev. D 105 (6) (2022) 063524, http://dx.doi.org/10.1103/PhysRevD.105.063524, arXiv:2106.02963.

[38] C. Krishnan, R. Mohayaee, E.O. Colgáin, M.M. Sheikh-Jabbari, L. Yin, Does hubble tension signal a breakdown in FLRW cosmology? Classical Quantum Gravity 38 (18) (2021) 184001, http://dx.doi.org/10.1088/1361-6382/ac1a81, arXiv:2105.09790.

[39] S. Vagnozzi, F. Pacucci, A. Loeb, Implications for the hubble tension from the ages of the oldest astrophysical objects, 2021, arXiv:2105.10421.

[40] A. Banerjee, H. Cai, L. Heisenberg, E.O. Colgáin, M.M. Sheikh-Jabbari, T. Yang, Hubble sinks in the low-redshift swampland, Phys. Rev. D 103 (8) (2021) L081305, http://dx.doi.org/10.1103/PhysRevD.103.L081305, arXiv:2006.00244.

[41] L. Heisenberg, H. Villarrubia-Rojo, J. Zosso, Can late-time extensions solve the H_0 and σ_8 tensions? 2022, arXiv:2202.01202.

[42] N. Banerjee, S. Das, K. Ganguly, Chameleon field and the late time acceleration of the universe, Pramana 74 (3) (2010) 481–489.

[43] S.K.J. Pacif, R. Myrzakulov, S. Myrzakul, Reconstruction of cosmic history from a simple parametrization of H, Int. J. Geom. Methods Mod. Phys. 14 (07) (2017) 1750111.

[44] S. Pacif, M.S. Khan, L. Paikroy, S. Singh, An accelerating cosmological model from a parametrization of Hubble parameter, Modern Phys. Lett. A 35 (05) (2020) 2050011.

[45] D. Blas, J. Lesgourgues, T. Tram, The cosmic linear anisotropy solving system (CLASS) II: Approximation schemes, J. Cosmol. Astropart. Phys. 1107 (2011) 034, http://dx.doi.org/10.1088/1475-7516/2011/07/034, arXiv:1104.2933.

[46] J. Lesgourgues, The cosmic linear anisotropy solving system (CLASS) III: Comparision with CAMB for LambdaCDM, 2011, arXiv:1104.2934.
[47] J. Lesgourgues, T. Tram, The cosmic linear anisotropy solving system (CLASS) IV: efficient implementation of non-cold relics, J. Cosmol. Astropart. Phys. 1109 (2011) 032, http://dx.doi.org/10.1088/1475-7516/2011/09/032, arXiv:1104.2935.
[48] T. Brinckmann, J. Lesgourgues, MontePython 3: boosted MCMC sampler and other features, 2018, arXiv:1804.07261.
[49] B. Audren, J. Lesgourgues, K. Benabed, S. Prunet, Conservative constraints on early cosmology: an illustration of the Monte python cosmological parameter inference code, J. Cosmol. Astropart. Phys. 1302 (2013) 001, http://dx.doi.org/10.1088/1475-7516/2013/02/001, arXiv:1210.7183.
[50] N. Roy, A.X. Gonzalez-Morales, L.A. Urena-Lopez, New general parametrization of quintessence fields and its observational constraints, Phys. Rev. D98 (6) (2018) 063530, http://dx.doi.org/10.1103/PhysRevD.98.063530, arXiv:1803.09204.
[51] N. Roy, K. Bamba, Arbitrariness of potentials in interacting quintessence models, Phys. Rev. D 99 (12) (2019) 123520, http://dx.doi.org/10.1103/PhysRevD.99.123520, arXiv:1811.03234.
[52] D.M. Scolnic, et al., The complete light-curve sample of spectroscopically confirmed SNe ia from pan-STARRS1 and cosmological constraints from the combined pantheon sample, Astrophys. J. 859 (2) (2018) 101, http://dx.doi.org/10.3847/1538-4357/aab9bb, arXiv:1710.00845.
[53] S. Alam, M. Ata, S. Bailey, F. Beutler, D. Bizyaev, J.A. Blazek, A.S. Bolton, J.R. Brownstein, A. Burden, C.-H. Chuang, et al., The clustering of galaxies in the completed SDSS-III baryon oscillation spectroscopic survey: cosmological analysis of the DR12 galaxy sample, Mon. Not. R. Astron. Soc. 470 (3) (2017) 2617–2652, http://dx.doi.org/10.1093/mnras/stx721.
[54] F. Beutler, C. Blake, M. Colless, D.H. Jones, L. Staveley-Smith, L. Campbell, Q. Parker, W. Saunders, F. Watson, The 6dF Galaxy Survey: baryon acoustic oscillations and the local Hubble constant, Mon. Not. R. Astron. Soc. 416 (4) (2011) 3017–3032, http://dx.doi.org/10.1111/j.1365-2966.2011.19250.x.
[55] A. Cuceu, J. Farr, P. Lemos, A. Font-Ribera, Baryon acoustic oscillations and the hubble constant: past, present and future, J. Cosmol. Astropart. Phys. 2019 (10) (2019) 044, http://dx.doi.org/10.1088/1475-7516/2019/10/044.
[56] E.A. Kazin, J. Koda, C. Blake, N. Padmanabhan, S. Brough, M. Colless, C. Contreras, W. Couch, S. Croom, D.J. Croton, et al., The WiggleZ dark energy survey: improved distance measurements to z = 1 with reconstruction of the baryonic acoustic feature, Mon. Not. R. Astron. Soc. 441 (4) (2014) 3524–3542, http://dx.doi.org/10.1093/mnras/stu778.
[57] A.J. Ross, L. Samushia, C. Howlett, W.J. Percival, A. Burden, M. Manera, The clustering of the SDSS DR7 main Galaxy sample – I. A 4 per cent distance measure at z = 0.15, Mon. Not. R. Astron. Soc. 449 (1) (2015) 835–847, http://dx.doi.org/10.1093/mnras/stv154.
[58] M. Tegmark, D.J. Eisenstein, M.A. Strauss, D.H. Weinberg, M.R. Blanton, J.A. Frieman, M. Fukugita, J.E. Gunn, A.J.S. Hamilton, G.R. Knapp, et al., Cosmological constraints from the SDSS luminous red galaxies, Phys. Rev. D 74 (12) (2006) http://dx.doi.org/10.1103/physrevd.74.123507.
[59] N. Arendse, R.J. Wojtak, A. Agnello, G.C.-F. Chen, C.D. Fassnacht, D. Sluse, S. Hilbert, M. Millon, V. Bonvin, K.C. Wong, et al., Cosmic dissonance: are new physics or systematics behind a short sound horizon? Astron. Astrophys. 639 (2020) A57, http://dx.doi.org/10.1051/0004-6361/201936720.
[60] J.A. Vázquez, D. Tamayo, A.A. Sen, I. Quiros, Bayesian model selection on scalar ϵ-field dark energy, Phys. Rev. D 103 (4) (2021) 043506, http://dx.doi.org/10.1103/PhysRevD.103.043506, arXiv:2009.01904.
[61] F.X. Linares Cedeño, N. Roy, L.A. Ureña López, Tracker phantom field and a cosmological constant: Dynamics of a composite dark energy model, Phys. Rev. D 104 (12) (2021) 123502, http://dx.doi.org/10.1103/PhysRevD.104.123502, arXiv:2105.07103.
[62] A.G. Riess, S. Casertano, W. Yuan, L.M. Macri, D. Scolnic, Large magellanic cloud cepheid standards provide a 1% foundation for the determination of the hubble constant and stronger evidence for physics beyond ΛCDM, Astrophys. J. 876 (1) (2019) 85, http://dx.doi.org/10.3847/1538-4357/ab1422, arXiv:1903.07603.
[63] S. Alam, et al., The clustering of galaxies in the completed SDSS-III baryon oscillation spectroscopic survey: cosmological analysis of the DR12 galaxy sample, Mon. Not. R. Astron. Soc. 470 (3) (2017) 2617–2652, http://dx.doi.org/10.1093/mnras/stx721, arXiv:1607.03155.
[64] P. Zarrouk, et al., The clustering of the SDSS-IV extended baryon oscillation spectroscopic survey DR14 quasar sample: measurement of the growth rate of structure from the anisotropic correlation function between redshift 0.8 and 2.2, Mon. Not. R. Astron. Soc. 477 (2) (2018) 1639–1663, http://dx.doi.org/10.1093/mnras/sty506, arXiv:1801.03062.
[65] M. Blomqvist, et al., Baryon acoustic oscillations from the cross-correlation of Lyα absorption and quasars in eBOSS DR14, Astron. Astrophys. 629 (2019) A86, http://dx.doi.org/10.1051/0004-6361/201935641, arXiv:1904.03430.
[66] V. de Sainte Agathe, et al., Baryon acoustic oscillations at z = 2.34 from the correlations of Lyα absorption in eBOSS DR14, Astron. Astrophys. 629 (2019) A85, http://dx.doi.org/10.1051/0004-6361/201935638, arXiv:1904.03400.
[67] R. Trotta, Applications of Bayesian model selection to cosmological parameters, Mon. Not. R. Astron. Soc. 378 (2007) 72–82, http://dx.doi.org/10.1111/j.1365-2966.2007.11738.x, arXiv:astro-ph/0504022.
[68] A. Heavens, Y. Fantaye, A. Mootoovaloo, H. Eggers, Z. Hosenie, S. Kroon, E. Sellentin, Marginal likelihoods from Monte Carlo Markov chains, 2017, arXiv:1704.03472.
[69] N. Aghanim, et al., Planck 2018 results. V. CMB power spectra and likelihoods, Astron. Astrophys. 641 (2020) A5, http://dx.doi.org/10.1051/0004-6361/201936386, arXiv:1907.12875.
[70] B.A. Reid, et al., Cosmological constraints from the clustering of the sloan digital sky survey DR7 luminous red galaxies, Mon. Not. R. Astron. Soc. 404 (2010) 60–85, http://dx.doi.org/10.1111/j.1365-2966.2010.16276.x, arXiv:0907.1659.
[71] B. Abolfathi, et al., The fourteenth data release of the sloan digital sky survey: First spectroscopic data from the extended baryon oscillation spectroscopic survey and from the second phase of the apache point observatory galactic evolution experiment, Astrophys. J. Suppl. 235 (2) (2018) 42, http://dx.doi.org/10.3847/1538-4365/aa9e8a, arXiv:1707.09322.
[72] M.A. Troxel, et al., Dark energy survey year 1 results: Cosmological constraints from cosmic shear, Phys. Rev. D 98 (4) (2018) 043528, http://dx.doi.org/10.1103/PhysRevD.98.043528, arXiv:1708.01538.
[73] S. Chabanier, M. Millea, N. Palanque-Delabrouille, Matter power spectrum: from Lyα forest to CMB scales, Mon. Not. R. Astron. Soc. 489 (2) (2019) 2247–2253, http://dx.doi.org/10.1093/mnras/stz2310, arXiv:1905.08103.
[74] L.A. Ureña López, N. Roy, Generalized tracker quintessence models for dark energy, Phys. Rev. D 102 (6) (2020) http://dx.doi.org/10.1103/physrevd.102.063510.
[75] W. Fang, W. Hu, A. Lewis, Crossing the phantom divide with parameterized post-friedmann dark energy, Phys. Rev. D 78 (2008) 087303, http://dx.doi.org/10.1103/PhysRevD.78.087303, arXiv:0808.3125.
[76] R.C. Nunes, S. Vagnozzi, S. Kumar, E. Di Valentino, O. Mena, New tests of dark sector interactions from the full-shape galaxy power spectrum, 2022, arXiv e-prints, arXiv:2203.08093.